

# Optimal Aluminum Doping Method in PEALD for Designing Outstandingly Stable InAlZnO TFT

Namgyu Woo, Seong-In Cho, and Sang-Hee Ko Park\*

Oxide semiconductors are promising semiconducting materials for next-generation thin-film transistors (TFTs). The role of the cations should be considered in the design of oxide semiconductors suitable for various applications. Ga has been widely used as a carrier suppressor in oxide semiconductors; however, research has recently been conducted to replace it with Al, which is cheaper and forms a stronger bond with O. Deposition using plasma-enhanced atomic layer deposition (PEALD) is very useful for controlling the composition of the cations in an oxide semiconductor. In this study, an InAlZnO (IAZO) semiconductor was deposited using super-cycle PEALD for the first time. Al<sub>2</sub>O<sub>3</sub> (AO), AlZnO (AZO), and InAlO (IAO) as Al doping layers in IAZO are evaluated. Considering its electrical characteristics and stability, AZO is selected as the optimal Al doping layer. The IAZO thin film and TFT characteristics according to the Al doping method are examined through the role of the cations and H concentration. In addition, the Al concentration is controlled by adjusting the number of cycles in super-cycle PEALD. As the Al concentration decreased, the mobility increased; however, the stability degraded significantly, which is induced by the increase in oxygen vacancies. Finally, the high-Al IAZO system using AZO successfully showed overall excellent properties including mobility over 10 cm<sup>2</sup> V<sup>-1</sup> s, and outstanding stability under 0.1 V, which are greatly improved compared to previously reported IAZO TFTs.

In particular, the high mobility of oxide semiconductors compared to amorphous Si (a-Si) is suitable for achieving high-resolution, high-driving frequency displays, and the amorphous phase of oxide semiconductors can solve the issues caused by grain boundaries, which is a fatal problem of low-temperature poly-Si (LTPS).<sup>[3–6]</sup> In addition, because oxide semiconductors have high back-end-of-line (BEOL) compatibility, research on their application in memory devices is also actively progressing.<sup>[7]</sup> The extremely low off-current of oxide semiconductors can improve the retention of dynamic random-access memory (DRAM)<sup>[8,9]</sup> by lowering the charge loss through the transistor, and oxide semiconductors exhibit good compatibility with various insulating layers, allowing them to be used as semiconductor materials for NAND flash<sup>[10,11]</sup> or ferroelectric random-access memory (FeRAM).<sup>[12]</sup>

For these various applications of oxide semiconductors, it is important to understand the role of the elements in oxide semiconductors to optimize the characteristics of thin films and devices. In particular, the characteristics of the devices can vary dramatically depending on the ratio of the cations in the oxide semiconductors.

In the case of InGaZnO (IGZO), a representative quaternary oxide semiconductor, the role of each cation composition is already known, and studies are being conducted to determine their optimal composition.<sup>[4,13–16]</sup> It is known to form a path for electrons to move through a large sphere-shaped 5s orbital.<sup>[14]</sup> Therefore, as the composition ratio of In increases, mobility increases; however, stability can be degraded owing to weak bonding between In and O. Moreover, Zn contributes to the formation of a network of oxide semiconductors. Finally, Ga is known as a carrier suppressor and long-range stabilizer of IGZO.<sup>[1]</sup> Ga<sup>3+</sup> forms a stronger chemical bond with O<sup>2-</sup> than with Zn<sup>2+</sup> or In<sup>3+</sup>; therefore, the oxygen vacancy (V<sub>O</sub>), which is one of the reasons for carrier formation and instability, can be suppressed.<sup>[17]</sup> However, several issues with IGZO arise from this Ga composition. For a carrier suppressor, the binding energy between Ga and O is weak, and IGZO has a relatively narrow band gap, which causes instability under illumination.<sup>[18,19]</sup> Additionally, inexpensive carrier suppressor elements that can replace relatively expensive Ga are required. From these points of view, research on InAlZnO (IAZO) using Al as a replacement element for Ga is being conducted.<sup>[20–22]</sup>

## 1. Introduction

Oxide semiconductors, which exist in the form of oxidized metals, are being actively researched as promising semiconductor materials in applications including displays, memory devices, and sensors owing to their various electrical advantages.<sup>[1]</sup> For display applications, active research has been conducted on the use of oxide semiconductor thin-film transistors (TFTs) as the driving components of next-generation displays.<sup>[2]</sup>

N. Woo, S.-I. Cho, S.-H. K. Park  
 Department of Materials Science and Engineering  
 Korea Advanced Institute of Science and Technology (KAIST)  
 291 Daehak-ro, Yuseong-gu, Daejeon 305–701, Republic of Korea  
 E-mail: shkp@kaist.ac.kr

 The ORCID identification number(s) for the author(s) of this article can be found under <https://doi.org/10.1002/admi.202300128>.

© 2023 The Authors. Advanced Materials Interfaces published by Wiley-VCH GmbH. This is an open access article under the terms of the Creative Commons Attribution License, which permits use, distribution and reproduction in any medium, provided the original work is properly cited.

DOI: 10.1002/admi.202300128

As the binding energy of Al-O ( $502 \text{ kJ mol}^{-1}$ ) is larger than that of Ga-O ( $374 \text{ kJ mol}^{-1}$ ), Al can better suppress the formation of  $V_o$ .<sup>[23,24]</sup> According to previous reports, owing to its strong binding energy, IAZO has a larger band gap ( $\approx 4.1 \text{ eV}$ ) than that of IGZO ( $\approx 3.2 \text{ eV}$ ).<sup>[24,25]</sup> In addition, Al is one of the most abundant elements on Earth, and it is also low-cost.<sup>[26]</sup> Unfortunately, the performances of IAZO TFTs reported so far generally have shown a lower mobility than IGZO ( $\approx 10 \text{ cm}^2 \text{ V}^{-1} \text{ s}^{-1}$ ) or deteriorated stability because there has been no fine control of the amount of Al.<sup>[27]</sup>

As mentioned above, because each cation of a quaternary oxide semiconductor has an individual role, the ratio of the elements should be precisely controlled to design the oxide semiconducting thin film. However, sputtering, which is the most common method for depositing an oxide semiconductor, is not suitable for this purpose. In the case of sputtering, it is difficult to change the composition of the thin film once the composition of the target is determined. Although the oxygen partial pressure can be controlled through reactive sputtering, it is not easy to control the ratio of cations through the oxygen partial pressure. In addition, by utilizing the cosputtering method, which uses multiple targets, it is possible to control the cation ratio; however, very fine control is still difficult. Conversely, only one atomic layer is deposited by one cycle of plasma-enhanced atomic layer deposition (PEALD),<sup>[28]</sup> and it is very easy to fine-tune the composition ratio of the oxide thin film.<sup>[14,29,30]</sup> In particular, the super-cycle PEALD method, in which each atomic layer is deposited alternately, can control the ratio of elements in the thin film by adjusting the ratio of the number of cycles of the atomic layer. Therefore, PEALD can provide an excellent method to inject Al into IAZO and control its amount. However, to the best of our knowledge, there has been no research on IAZO thin film deposition or IAZO TFT fabrication through PEALD.<sup>[25]</sup>

Here, we designed an IAZO thin film by successfully investigating the effect of the Al doping method and the amount of Al. In particular, super-cycle PEALD was used for the first time for IAZO deposition. We compared the properties of IAZO thin films and IAZO TFTs when  $\text{Al}_2\text{O}_3$  (AO),  $\text{AlZnO}$  (AZO), and  $\text{InAlO}$  (IAO) were used as Al doping layers, and we confirmed that Al doping using AZO was the optimal method. In addition,

the characteristics and defects of the IAZO TFTs with respect to the Al concentration were investigated by adjusting the cycle ratio of the super-cycle. PEALD-processed IAZO-based TFT showed extraordinary stability under positive bias temperature stress (PBTs) conditions with a mobility of over  $10 \text{ cm}^2/\text{V}\cdot\text{s}$ , which is comparable to that of IGZO. This was an excellent characteristic compared with previously reported IAZO TFTs, and it was possible because of the fine control of Al through PEALD.

## 2. Results and Discussion

### 2.1. Effect of the Al Doping Method Through PEALD on IAZO TFTs

Three types of Al doping layers can be considered for IAZO deposition:  $\text{Al}_2\text{O}_3$ , homogeneous-AZO (homo-AZO), and homogeneous-IAO (homo-IAO). Because the composition of the entire IAZO will differ according to each doping method and the electrical properties of the devices are expected to differ accordingly, the effects of the three types of Al doping layers were investigated. In this study, the deposited IAZO thin films by doping with  $\text{Al}_2\text{O}_3$ , AZO, and IAO were named AO-IAZO, AZO-IAZO, and IAO-IAZO, respectively. **Figure 1a** shows a schematic of the PEALD of IAZO using the super-cycle method. One super-cycle for IAZO deposition was composed of  $\{[(\text{In}_2\text{O}_3 \text{ 5 cy}) + (\text{ZnO 1 cy})] \times 3 + (\text{Al}_2\text{O}_3, \text{AZO, or IAO 1 cy})\}$ . To observe the atomic percentages of the IAZO thin films, an XPS depth profile was conducted (**Figure 1b–d**). Regardless of the Al doping method, all three films exhibited uniform compositions according to the etching time. The chemical compositions determined by XPS are listed in Table S1, Supporting Information. According to XPS, AO-IAZO showed the highest Al concentration, and AZO-IAZO showed the lowest Al concentration. In addition, IAO-IAZO and AZO-IAZO exhibited the highest In and Zn concentrations, respectively. **Figure 1e–g** shows the atomic compositions of  $\text{Al}_2\text{O}_3$ , homo-AZO, and homo-IAO obtained via RBS analysis. It was confirmed that all three layers contained Al, and they could act as Al doping layers.

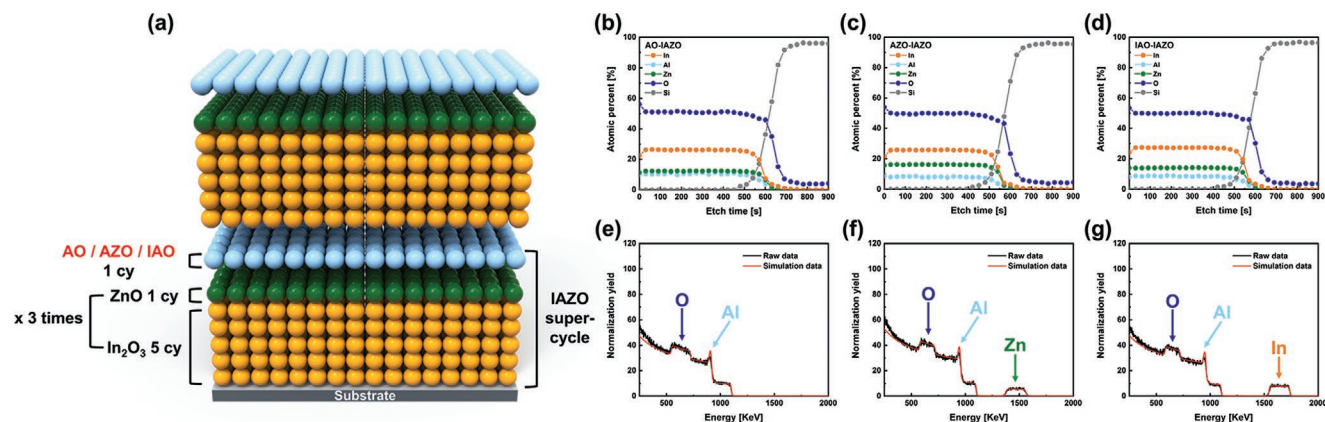


**Figure 1.** a) Schematic of the super-cycle PEALD of IAZO thin films with AO, AZO, and IAO. Atomic distribution via the XPS depth profiles of b) AO-IAZO, c) AZO-IAZO, and d) IAO-IAZO. RBS-based element detection of e)  $\text{Al}_2\text{O}_3$ , f) homo-AZO, and g) homo-IAO.

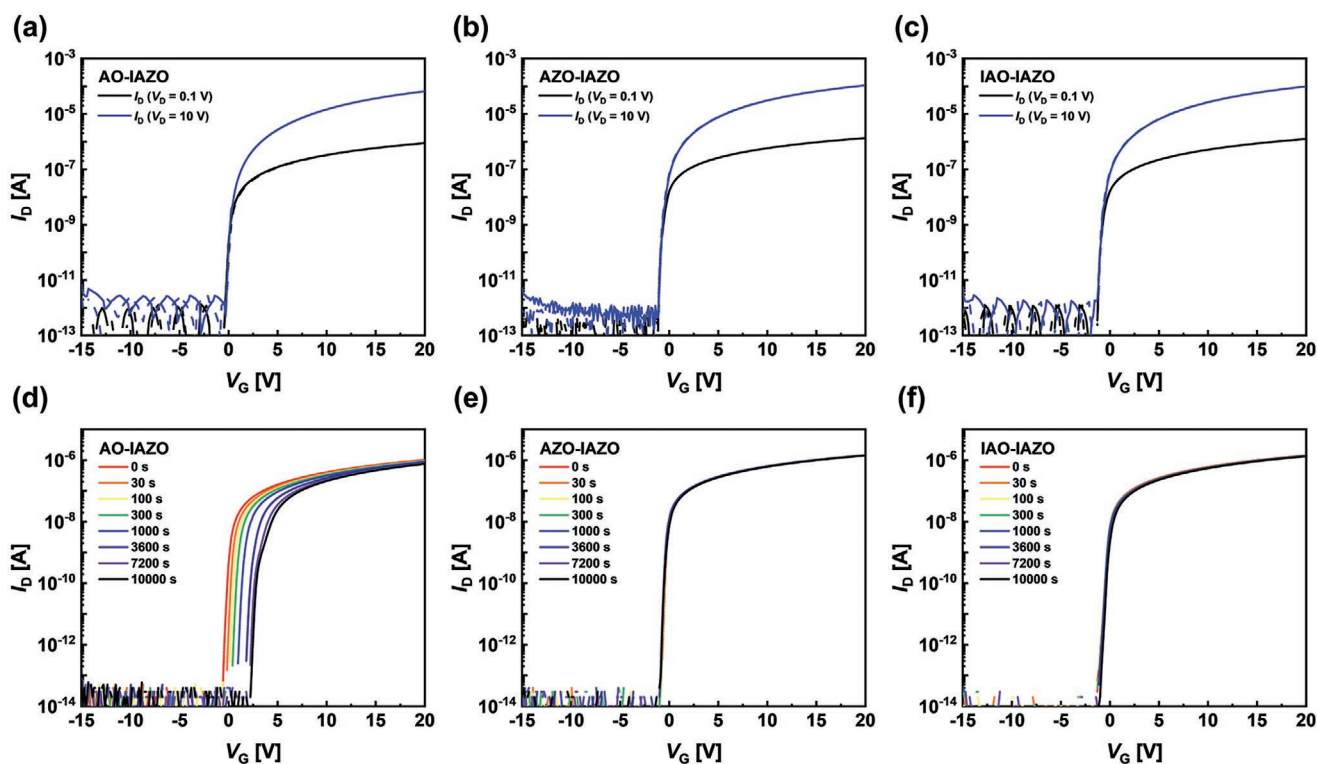


**Figure 2.** Transfer curves of the fabricated TFTs based on a) AO-IAZO, b) AZO-IAZO, and c) IAO-IAZO. The solid and dashed lines represent forward and backward sweeps, respectively. PBTs stability results of TFTs based on d) AO-IAZO, e) AZO-IAZO, and f) IAO-IAZO.

The transfer curves of the fabricated IAZO TFTs with different Al doping methods are shown in Figure 2a–c, and their electrical characteristics are summarized in Table 1. The structures, materials, and processes are shown in Figure S1, Supporting Information. Almost no hysteresis (hys) was observed for any of the three IAZO TFTs. In general, as the concentration of Al increases, the mobility of the TFT decreases and the  $V_{on}$  value shifts to positive values.<sup>[26]</sup> This is because Al suppresses the generation of  $V_0$ , which is the donor of the oxide semiconductor, and the carrier concentration decreases. The mobilities of the three IAZO TFTs can be clearly explained by the role of Al. As mentioned in the results of the XPS depth profile (Figure 1b–d), AZO-, IAO-, and AO-IAZO showed increasingly high Al contents in that order. In addition, the measured mobility also showed low values. AO-IAZO TFT showed a low mobility of  $7.56 \text{ cm}^2 \text{ V}^{-1} \text{ s}^{-1}$ , which is also low compared to general IGZO with a mobility of  $\approx 10 \text{ cm}^2 \text{ V}^{-1} \text{ s}^{-1}$ . Conversely, both AZO- and IAO-IAZO TFTs showed mobilities above  $10 \text{ cm}^2 \text{ V}^{-1} \text{ s}^{-1}$ , which indicates that they can replace IGZO. The AZO-IAZO TFT showed slightly higher mobility

**Table 1.** Electrical properties of each IAZO TFT according to the Al doping method.

| Al doping method   | AO-IAZO          | AZO-IAZO         | IAO-IAZO         |
|--|------------------|------------------|------------------|
| Mobility [ $\text{cm}^2 \text{ V}^{-1} \text{ s}^{-1}$ ] | $7.56 \pm 0.21$  | $10.81 \pm 0.46$ | $10.29 \pm 0.38$ |
| Subthreshold-swing [V per decade]                        | $0.12 \pm 0.03$  | $0.11 \pm 0.02$  | $0.13 \pm 0.02$  |
| $V_{on}$ [V]   | $-0.30 \pm 0.08$ | $-1.04 \pm 0.33$ | $-1.47 \pm 0.22$ |

than the IAO-IAZO TFT, which seems to be due to the relatively low Al content. Meanwhile,  $V_{on}$  cannot be explained only by the Al concentration because the concentration of In or Zn and the concentration of Al changed as the doping method changed. A higher In concentration is known to induce a negative  $V_{on}$  value because of the weak bonding between In and O.<sup>[14]</sup> In fact, the IAO-IAZO TFT in which In was detected the most via XPS had the most negative  $V_{on}$  value, and the AO-IAZO TFT with a high Al content had the most positive  $V_{on}$  value. In terms of electrical characteristics, AZO appears to be the best Al doping layer. The AZO-IAZO TFT showed high mobility when compared with IGZO or the previously reported IAZO, and the  $V_{on}$  value was suitable. Figure S2, Supporting Information, shows the output curves of the AZO-IAZO TFT. It was confirmed that there was no contact issue between the source/drain (S/D) electrodes and IAZO.

Figure 2d–f shows the PBTs stability of the IAZO TFTs according to the Al doping method. According to previous studies, the higher the Al content, the better the stability of PBTs. Generally, ionized  $V_0$  ( $V_0^+$  or  $V_0^{++}$ ) can trap free electrons, which is the main mechanism of PBTs instability,<sup>[31,32]</sup> and can also be suppressed by Al; therefore, Al can improve the PBTs stability of oxide TFTs. However, the three IAZO TFTs showed opposite results. For the AO-IAZO TFT, the worst PBTs stability of 2.93 V shifting of  $V_{on}$  occurred. In addition,  $V_{on}$  of the IAO-IAZO TFT was shifted 0.16 V under the PBTs condition. In contrast, the  $V_{on}$  of the AZO-IAZO TFT hardly shifted ( $< 0.1 \text{ V}$ ) and showed outstanding PBTs stability.

Because these PBTs stability results are difficult to explain in terms of the role of Al, it should be suspected that the Al doping

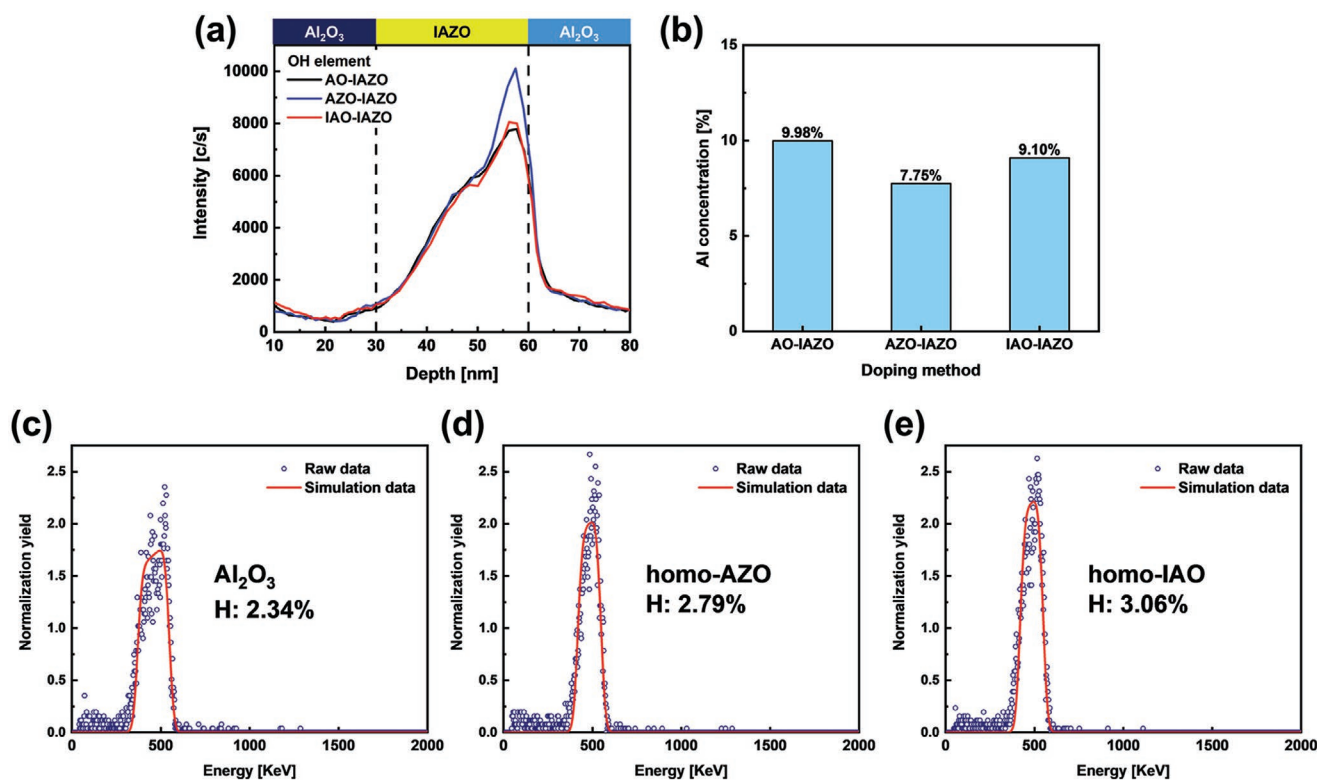


**Figure 3.** a) OH inside of Al<sub>2</sub>O<sub>3</sub>/IAZO/Al<sub>2</sub>O<sub>3</sub> detected by SIMS analysis. b) Al concentration of each IAZO thin film was determined using RBS. H concentration using ERD for c) Al<sub>2</sub>O<sub>3</sub>, b) homo-AZO, and e) homo-IAO.

method has another effect. In particular, as the Al doping layer was changed, the H content of the IAZO changed accordingly. H inside of the oxide semiconductor is a very important element that can passivate defects.<sup>[31,33,34]</sup> The amount of H according to the Al doping method can be a factor determining the PBTS stability. The hydroxyl group (OH) inside of Al<sub>2</sub>O<sub>3</sub>/IAZO/Al<sub>2</sub>O<sub>3</sub> detected by secondary ion mass spectroscopy (SIMS) is shown in **Figure 3a**. The Al<sub>2</sub>O<sub>3</sub> layer on IAZO mimics the passivation and protection layers (PL), and the Al<sub>2</sub>O<sub>3</sub> layer under IAZO mimics the gate insulator (GI). According to the SIMS results, the most OH was present in AZO-IAZO, which had the best stability, and the least OH was present in AO-IAZO, which had the most degraded stability. This is because the amount of H as a defect passivator differed depending on the Al doping method, and the stability improved as more H was present. Two reasons can be considered because the amount of H varies according to the doping method: 1) the incorporation of external H changes; 2) the amount of H in IAZO differed.<sup>[31,35]</sup> To verify the reason related to the presence of external H, the Al concentrations of the IAZO thin films were verified through RBS (**Figure 3b**). Although the detailed values were slightly different, the Al concentration was increasingly high in the order of AZO-, IAO-, and AO-IAZO, similar to the XPS depth profile results. Al-based oxide thin films are known to have lower H permeability than other oxide thin films.<sup>[36,37]</sup> This is due to the high density of the Al-based oxide thin films. Even in the case of IAZO according to this doping method, AZO-IAZO contained the lowest amount of Al, and it is possible that more H was introduced from the outside, including the GI, PL, and pas-

sivation layers. In addition, to confirm the possibility that the amount of H in the thin film itself changed according to the Al doping method, the amount of H in Al<sub>2</sub>O<sub>3</sub>, AZO, and IAO was confirmed through ERD (**Figure 3c–e**). Some H impurities from the metal precursors can remain owing to an incomplete reaction between the precursors and the oxygen reactant.<sup>[34,35]</sup> The H concentrations in the Al doping layers were slightly different. Al<sub>2</sub>O<sub>3</sub> showed the lowest H concentration of 2.34%, which was the same result as that provided via SIMS (**Figure 3a**). AZO (2.79%) and IAO (3.06%) contained higher amounts of H than Al<sub>2</sub>O<sub>3</sub>, but the differences were not significant. Therefore, it seems that the amount of H in the thin film itself has an effect, but it is difficult to interpret the SIMS and PBTS results using only the second reason. Because of the lower H concentration in Al<sub>2</sub>O<sub>3</sub> and the lower H permeability due to the high Al concentration, the AO-IAZO TFT had less H in the active layer. This caused the AO-IAZO TFT to have deteriorated PBTS stability despite the high Al concentration. Conversely, AZO-IAZO was confirmed to have a high H concentration via SIMS, which is due to its high H permeability. The high H concentration of AZO-IAZO induced extraordinary PBTS stability despite its low Al concentration. The AZO-IAZO TFT had not only the best electrical characteristics but also outstanding reliability; therefore, we selected AZO as the optimal Al doping layer.

Finally, the subgap density of states (DOS) of each IAZO TFTs was extracted using the differential ideality factor technique (DIFT) method (**Figure 4**).<sup>[38]</sup> The subgap density in the oxide semiconductor determines the overall properties of the TFTs, including their electrical properties and stability.<sup>[39]</sup>

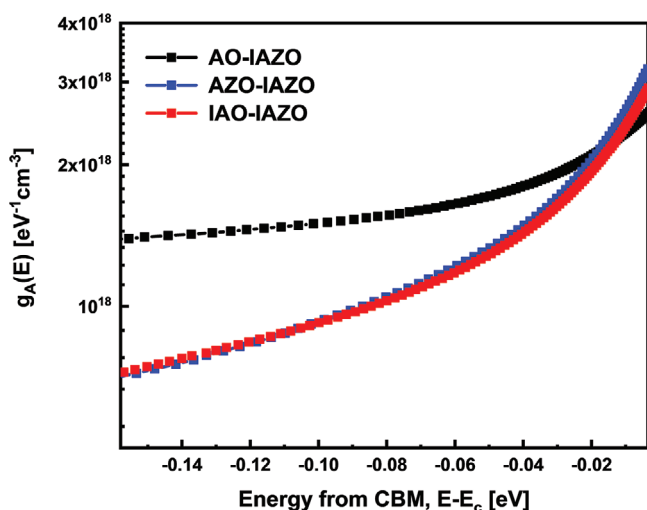


Figure 4. DOS of each IAZO TFT extracted from the DIFT method.

AO-IAZO showed a low DOS at the shallow level, which is strongly related to ionized  $V_o$  ( $V_o^+$ ,  $V_o^{++}$ ); however, it showed a high DOS at the deep level, which can be passivated by H.<sup>[39]</sup> Conversely, both AZO-IAZO and IAO-IAZO showed a low DOS at the deep state, resulting in high stability.

## 2.2. Effect of Al concentration on IAZO TFTs

Although we confirmed AZO as the optimal Al doping layer, the IAZO TFT can still be optimized by controlling the cycle ratio of the super-cycle to optimize the Al concentration. To investigate the effect of Al content on IAZO TFTs, the AZO-IAZO was deposited by varying the number of  $\text{In}_2\text{O}_3$  deposition cycles (5/7/10 cy) to control the Al content, as shown in Figure 5a. In this study, the deposited films were referred to as high Al- (HA-,  $\text{In}_2\text{O}_3$  5 cy), medium Al- (MA-,  $\text{In}_2\text{O}_3$  7 cy), and low Al-IAZO (LA-,  $\text{In}_2\text{O}_3$  10cy) depending on the Al concentration. Owing to a significant change in the Al concentration when the deposition cycle of AZO is altered, we adjusted the deposition cycle of  $\text{In}_2\text{O}_3$  to finely control the element ratio. XPS depth profile

analysis was performed to confirm the elemental composition of the IAZO thin films according to depth (Figure 5b–d). The atomic ratios according to the variation in the number of deposition cycles are shown in Table S2, Supporting Information. All the elements were uniformly deposited regardless of the deposition recipe, and the Al concentration varied according to the number of  $\text{In}_2\text{O}_3$  deposition cycles.

XRD was conducted to confirm the crystallinity of the HA, MA, and LA-IAZO thin films, as shown in Figure 5e. All IAZO films exhibited the same amorphous state even after the annealing process. Therefore, it can be said that the differences in the electrical characteristics of the IAZO TFTs to be discussed later do not arise from the crystallinity of the IAZO films. In addition, to confirm the wide band gap of IAZO, as mentioned in the introduction, the optical band gaps of the IAZO thin films were obtained by UV-vis analysis (Figure 5f). IAZO thin films have an optical band gap of  $\approx 4.9$  eV, which is much larger than the average band gap of IGZO ( $\approx 3.2$  eV).<sup>[18,19,21]</sup> The enlarged image shows that the optical band gap of IAZO also increases as the Al content increases. The wide band gap of  $\text{Al}_2\text{O}_3$ , induced by the strong bonding between Al and O, contributes to the wide band gap of IAZO. As a result, we confirmed that wide band gap tuning was possible by using Al instead of Ga.

The transfer curves of AZO-IAZO TFTs with different Al concentrations are shown in Figure 6a–c, and the electrical properties are shown in Table 2. Figure S3, Supporting Information, shows an illustration of the fabricated IAZO TFTs. All three TFTs exhibited almost no hys. They followed a typical trend according to the amount of Al.<sup>[26]</sup> As the Al concentration increased,  $V_{\text{on}}$  shifted in the positive direction and mobility decreased. This trend of  $V_{\text{on}}$  and mobility can be explained by carrier suppression by Al and the percolation mechanism of oxide semiconductors. LA-IAZO had a high mobility of over  $20 \text{ cm}^2 \text{ V}^{-1} \text{ s}^{-1}$  but showed the worst performance in terms of  $V_{\text{on}}$ . Otherwise, HA-IAZO TFT had proper  $V_{\text{on}}$  value with a decreased mobility of  $10.81 \text{ cm}^2 \text{ V}^{-1} \text{ s}^{-1}$ , but it is still comparable to the mobility of typical IGZO. As mentioned above, Al is a carrier suppressor that suppresses the generation of  $V_o$ , which is a well-known electron donor in oxide semiconductors. In addition,  $V_o$  may affect the subthreshold-swing of the TFTs. As

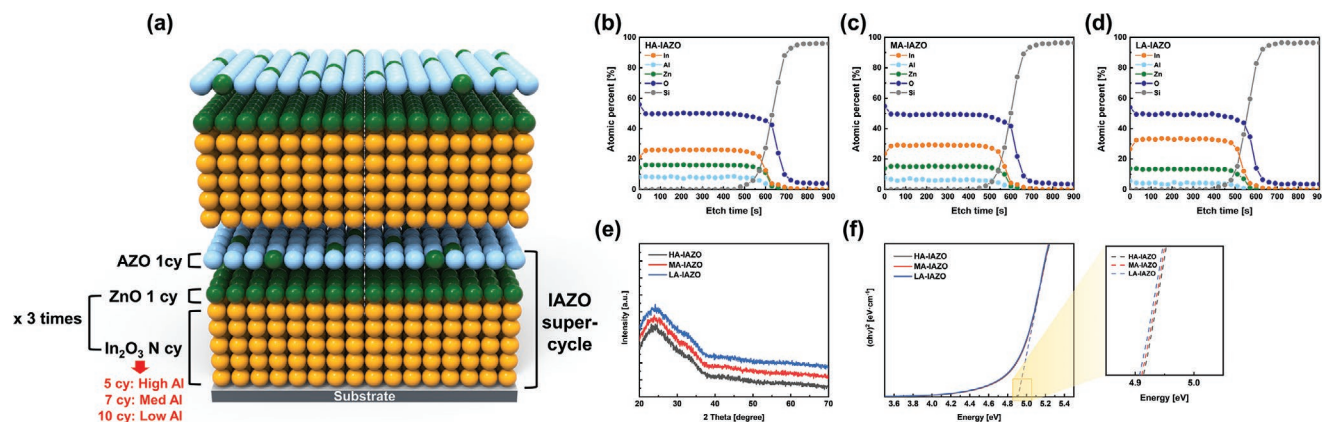
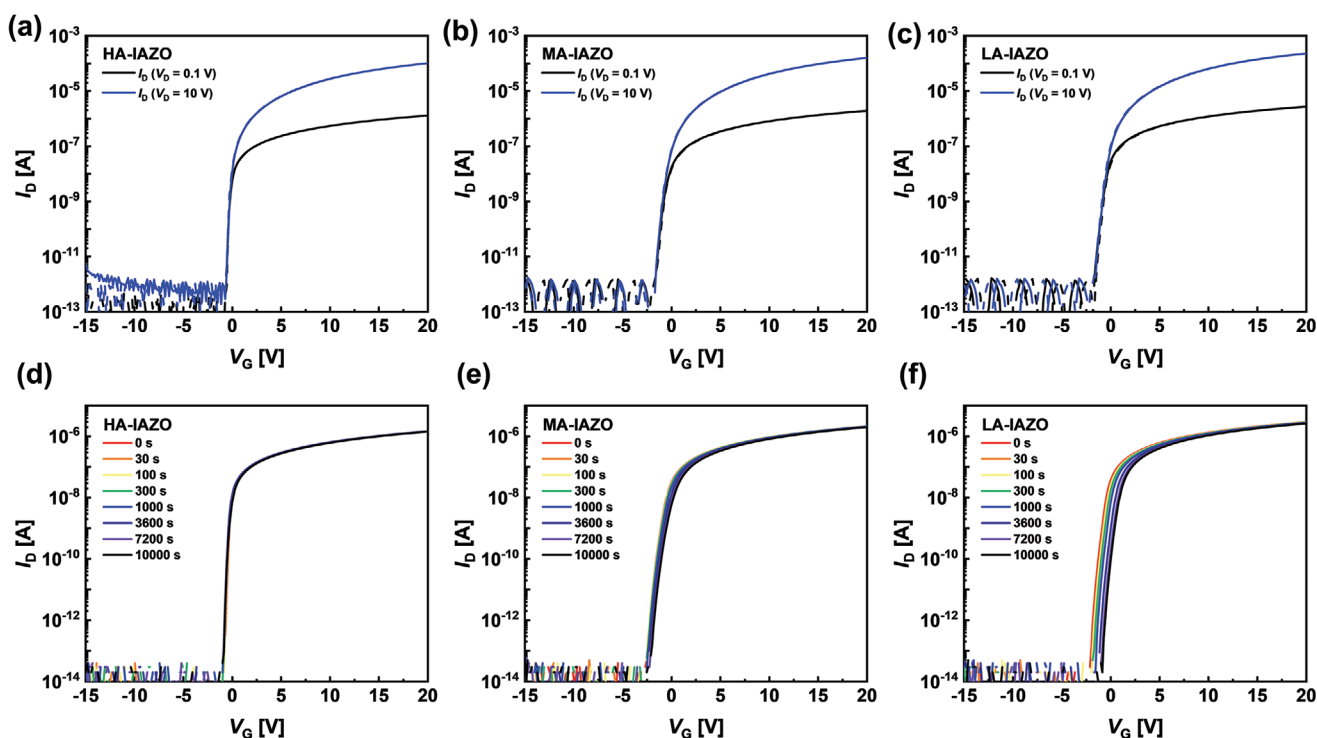


Figure 5. a) Schematic of the super-cycle PEALD of IAZO thin films with varying deposition cycles. Atomic distribution via the XPS depth profile of b) HA-IAZO, c) MA-IAZO, and d) LA-IAZO. e) XRD results of the IAZO thin films. f) Results of UV-vis analysis of the IAZO thin films.



**Figure 6.** Transfer curves of fabricated TFTs based on a) HA-IAZO, b) MA-IAZO, and c) LA-IAZO. The solid and dashed lines express forward and backward sweeps, respectively. Results of PBTS stability of the TFTs based on d) HA-IAZO, e) MA-IAZO, and f) LA-IAZO.

the concentration of Al increased, the subthreshold-swing value improved. Therefore, the differences in the electrical characteristics of the IAZO TFTs according to the Al in Figure 6a–c and Table 2 can be regarded as reasonable results.

Figure 6d–f shows the results of measuring the PBTS stability of IAZO TFTs with different Al contents. In HA-IAZO,  $V_{on}$  shift occurred by less than 0.1 V, and in MA- and LA-IAZO,  $V_{on}$  shift occurred in the positive direction by 0.48 and 1.27 V, respectively. As mentioned previously, the main factor degrading the PBTS stability is ionized  $V_o$  ( $V_o^+$  or  $V_o^{++}$ ), which traps free electrons.<sup>[39]</sup> Al has a much higher binding energy with O than other metal cations such as In and Zn; therefore, the higher the concentration of Al, the lower the amount of  $V_o$ .

XPS analysis was performed to verify the explanation of the electrical characteristics and PBTS stability using  $V_o$ . Figure 7a–c shows the result of the deconvolution of the HA-, MA-, and LA-IAZO O1s peaks through XPS analysis. The O1s peaks could be deconvoluted into metal-O (M–O),  $V_o$ , and OH.<sup>[20]</sup> The area occupied by  $V_o$  relative to the M–O bond was 0.25 for HA-IAZO, 0.34 for MA-IAZO, and 0.41 for LA-IAZO, and  $V_o$  tended to increase as the Al content decreased. This can

**Table 2.** Electrical properties of each IAZO TFT according to the Al doping concentration.

| Al concentration                                       | HA-IAZO          | MA-IAZO          | LA-IAZO          |
|--|------------------|------------------|------------------|
| Mobility [ $\text{cm}^2 \text{V}^{-1} \text{s}^{-1}$ ] | $10.81 \pm 0.46$ | $14.87 \pm 0.48$ | $20.56 \pm 0.47$ |
| Subthreshold-swing [V per decade]                      | $0.11 \pm 0.02$  | $0.27 \pm 0.01$  | $0.33 \pm 0.03$  |
| $V_{on}$ [V]   | $-1.04 \pm 0.33$ | $-1.32 \pm 0.12$ | $-1.70 \pm 0.32$ |

be easily determined by looking at the overlapped O1s peak in Figure S4, Supporting Information. As a result, it was confirmed that the trends of the PBTS stability and Al concentration in IAZO TFT coincided.

Figure 8 shows the results of the spectroscopic ellipsometer (SE) analysis used to confirm that  $V_o$  affected the DOS of IAZO. The imaginary dielectric function ( $\epsilon_2$ ) represents the light absorption by the subgap inside of the band gap.<sup>[24]</sup> The occurrence of light absorption indicates the presence of an electron trap site, which is directly related to the stability of PBTS.<sup>[31,40]</sup> The graph shows that the lower the Al content of IAZO, the higher the light absorption, which means that more electron trap sites are generated in LA-IAZO. Therefore, it can be concluded that the IAZO TFT reduces the PBTS stability because  $V_o$  is easily generated as the Al content decreases.

Considering the overall electrical properties, the HA-IAZO TFT doped with the AZO atomic layer was the optimized IAZO TFT with outstanding PBTS stability. Along with the IAZO TFTs in this study as well as the IAZO TFTs in the previously reported studies, the HA-AZO-IAZO TFTs showed excellent electrical parameters and extraordinary stability (Table 3). This was determined by investigating the effect of the Al doping layer and the concentration of Al due to PEALD. Because the PEALD process is more compatible and has a higher step coverage than other deposition methods, including plasma laser deposition (PLD) or solution-based processes, IAZO using PEALD can be used in a wide range of applications.<sup>[7]</sup> In addition, as shown in Figure S5, the manufactured IAZO TFTs are fully transparent; therefore, they can be applied to next-generation transparent electronic devices.

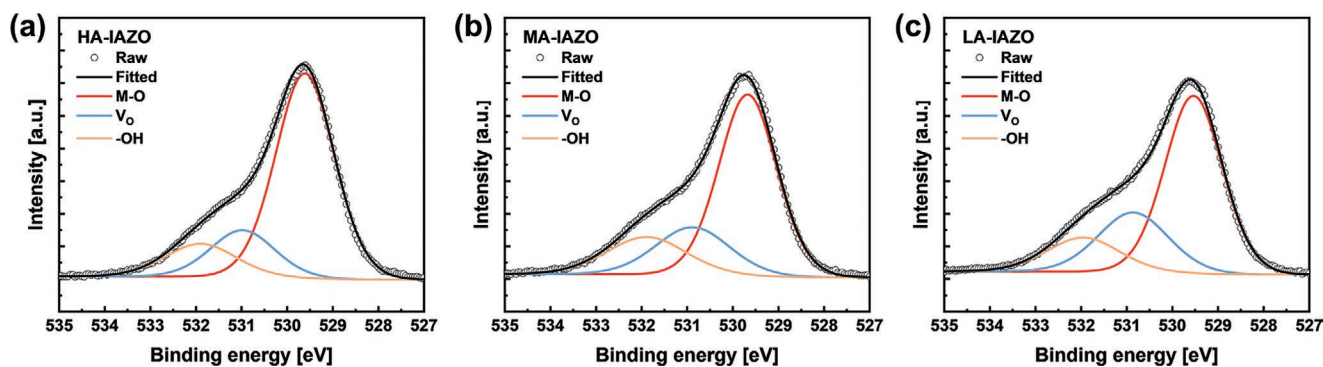


Figure 7. Deconvoluted O1s peaks of a) HA-, b) MA-, and c) LA-IAZO were detected by XPS.

### 3. Conclusion

The optimal Al doping method for IAZO deposition by PEALD and its effect on the IAZO TFT were investigated. AO-, AZO-, and IAO-IAZO were proposed as Al doping methods, and their electrical parameters and PBTS stability were measured by fabricating TFTs with each film. The difference in the electrical characteristics of each device was explained by the suppression of  $V_o$  by Al and the composition of metal cations, and the difference in the PBTS stability was analyzed through defect passivation by H. Among the three candidates, AZO-IAZO had the best TFT electrical parameters and reliability. Next, the effect of Al on IAZO was investigated by adjusting the cycle ratio of the AZO-IAZO recipe. Regardless of the amount of Al, all IAZO thin films appeared in an amorphous state. The optical band gap of the IAZO films was  $\approx 4.9$  eV wider than that of IGZO, and the size of the band gap also tended to increase as the Al content increased. In terms of the electrical parameters, the TFT mobility increased as the Al content decreased, but  $V_{on}$  moved in the negative direction. In addition, the TFT reliability tended to improve as the Al content increased, which was supported by XPS and SE analyses. Finally, a transparent

IAZO TFT with a high mobility comparable to IGZO and excellent stability was fabricated using PEALD for the first time, which can be applied to various semiconductor devices.

### 4. Experimental Section

**IAZO Thin Film Deposition Through PEALD:** IAZO films were deposited using showerhead-type PEALD equipment. [3-(dimethylamino)propyl] (dimethyl)indium (DADI), trimethylaluminum (TMA), and diethylzinc (DEZn) were used as ALD precursors for In, Al, and Zn. DADI was stored in a bubbler-type canister at 40 °C, and the other precursors were stored in single-valve canisters at room temperature. Oxygen plasma (100 W) was used as the reactant for the PEALD of IAZO. The  $O_2$  flow rate was maintained at 500 sccm during the PEALD process. Ar gas was used for purging (1000 sccm for DADI, 500 sccm for TMA and DEZn) and carrying gas (50 sccm for DADI, 500 sccm for TMA and DEZn).  $In_2O_3$  was deposited through {DADI 1 s–Ar 10 s– $O_2$  1 s–oxygen plasma 2 s–Ar 10 s}, and the  $Al_2O_3$  sequence was {TMA 0.1 s–Ar 10 s– $O_2$  1 s–oxygen plasma 2 s–Ar 10 s}. The ZnO layer was formed through {DEZn 0.1 s–Ar 10 s– $O_2$  1 s–oxygen plasma 2 s–Ar 10 s}. To deposit an atomic layer containing both Al and either In or Zn, the homogeneous method for PEALD was used. For homo-AZO and homo-IAO, the {DEZn or DADI 0.1 s– TMA 0.1 s–Ar 10 s– $O_2$  1 s–oxygen plasma 2 s–Ar 10 s} sequence was used (Figure S6, Supporting Information).

The chemical composition and  $V_o$  of IAZO according to depth were investigated using XPS (Nexa G2, Thermo Fisher Scientific Inc.). In

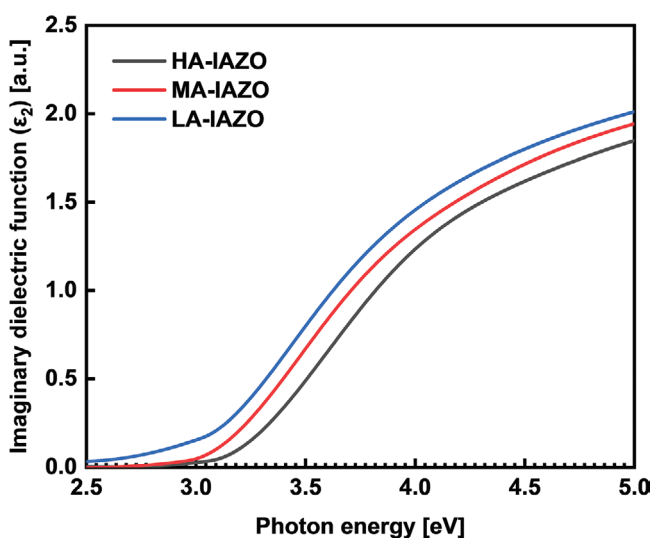


Figure 8. Imaginary dielectric function of IAZO according to the Al concentration extracted by SE analysis.

Table 3. Comparison of the electrical properties and stability between previously reported IAZO TFTs and the IAZO TFT in this work.

| Ref.      | Mobility [ $cm^2 V^{-1} s^{-1}$ ] | $V_{on}$ ( $V_{th}$ ) [V] | PBTS (PBS) stability [V] | Process       |
|-----------|-----------------------------------|---------------------------|--------------------------|---------------|
| [41]      | 2.2                               | $\approx 14$              | -                        | PLD           |
| [20]      | 2.2                               | 14                        | $\approx 2.5$ (10 000 s) | PLD           |
| [42]      | 0.66                              | -                         | 0.5 (10 000 s)           | sol-gel       |
| [43]      | 0.24                              | 1.65                      | -                        | sol-gel       |
| [21]      | 11.39                             | 0.32                      | $> 1$ (3000 s)           | sputtering    |
| [27]      | 5.67                              | 0.23                      | -                        | sputtering    |
| [25]      | 20.65                             | 6.34                      | 9.09 (hys)               | sputtering    |
| [44]      | 8.76                              | 6.32                      | 1.23 (hys)               | sputtering    |
| [26]      | 21.70                             | -2.24                     | 3.20 (7200 s)            | co-sputtering |
| [45]      | 7.64                              | 7.49                      | 5.81 (10 000 s)          | co-sputtering |
| This work | 10.81                             | -1.04                     | 0.095 (10 000 s)         | PEALD         |

addition, elements including H in these films were analyzed using RBS/ERD (NFC). SIMS (IMS7f) was used to detect the OH element inside the thin film stack. XRD (Ultima IV, Rigaku Co.) was also performed to investigate the phases of the IAZO thin films, and the optical band gap of IAZO was calculated using a UV-vis spectrophotometer (Lambda 1050, Perkin Elmer, Inc.). Finally, the imaginary dielectric function was extracted using SE analysis (M2000D, J.A. Woollam Co.).

**Fabrication Process of IAZO TFTs:** All thin films of the IAZO TFTs were patterned by photolithography and wet etching. To examine the IAZO semiconducting film, other factors were excluded, and bottom-gate bottom-contact (BGBC) structured TFTs were fabricated. First, a 150 nm-thick InSnO (ITO) layer on the glass substrate was used as the gate electrode. Then, Al<sub>2</sub>O<sub>3</sub> for GI was laminated to 185 nm by thermal ALD using H<sub>2</sub>O and TMA at 150 °C. ITO for the S/D electrodes was then again deposited at 150 nm by sputtering. Next, an IAZO active layer of 30 nm was placed on the S/D as previously described in the “IAZO thin film deposition through PEALD” section. The width and length of the patterned IAZO were 20 and 10 μm, respectively. A 10 nm-thick Al<sub>2</sub>O<sub>3</sub> layer deposited by PEALD was used for PL, which protects the active layer from chemical etchant and photoresist contamination. Finally, the TFTs were covered with Al<sub>2</sub>O<sub>3</sub> of 30 nm. The fabricated TFTs were annealed in a vacuum furnace to improve their properties.

The electrical properties of the fabricated IAZO TFTs were measured using a semiconductor parameter analyzer (HP4156A). The average value and standard deviation of the electrical properties were calculated for eight devices on the same sample. The PBTS stability was measured under a gate field of 1 MV/cm and a temperature of 60 °C for 10000 s.

## Supporting Information

Supporting Information is available from the Wiley Online Library or from the author.

## Acknowledgements

N.W. and S.-I.C. contributed equally to this work. This study was supported by the Ministry of Trade, Industry, and Energy (MOTIE, Korea) (20016319). This work was also supported by the Technology Development Program (S3207541), funded by the Ministry of SMEs and Startups (MSS, Korea).

## Conflict of Interest

The authors declare no conflict of interest.

## Data Availability Statement

Research data are not shared.

## Keywords

aluminum, InAlZnO, oxide semiconductors, plasma enhanced atomic layer deposition (PEALD), stability

Received: February 14, 2023

Revised: March 6, 2023

Published online:

[1] J. Troughton, D. Atkinson, *J. Mater. Chem. C* **2019**, *7*, 12388.

[2] H. J. Jang, J. Y. Lee, J. Kwak, D. Lee, J. H. Park, B. Lee, Y. Y. Noh, *J. Inform. Display* **2019**, *20*, 1.

- [3] E. Fortunato, P. Barquinha, R. Martins, *Adv. Mater.* **2012**, *24*, 2945.
- [4] J. S. Park, W. J. Maeng, H. S. Kim, J. S. Park, *Thin Solid Films* **2012**, *520*, 1679.
- [5] K. Nomura, H. Ohta, A. Takagi, T. Kamiya, M. Hirano, H. Hosono, *Nature* **2004**, *432*, 488.
- [6] A. J. Snell, W. E. Spear, P. G. Lecomber, K. Mackenzie, *Appl. Phys. A Mater.* **1981**, *26*, 83.
- [7] S. J. Ding, X. H. Wu, *Chem. Mater.* **2020**, *32*, 1343.
- [8] G. P. Yan, H. Yang, W. B. Liu, N. Zhou, Y. P. Hu, Y. F. Shi, J. F. Gao, G. L. Tian, Y. D. Zhang, L. J. Fan, G. L. Wang, G. B. Xu, J. S. Bi, H. X. Yin, C. Zhao, J. Luo, *IEEE Trans. Electron. Devices* **2022**, *69*, 2417.
- [9] X. L. Duan, K. L. Huang, J. X. Feng, J. B. Niu, H. B. Qin, S. H. Yin, G. F. Jiao, D. Leonelli, X. X. Zhao, Z. G. Wang, W. L. Jing, Z. B. Wang, Y. Wu, J. Xu, Q. Chen, X. C. Chuai, C. Y. Lu, W. W. Wang, G. H. Yang, D. Geng, L. Li, M. Liu, *IEEE Trans. Electron. Devices* **2022**, *69*, 2196.
- [10] H. Ji, Y. H. Wei, X. L. Zhang, R. Jiang, *Appl. Phys. Lett.* **2017**, *111*.
- [11] E. S. Hwang, J. S. Kim, S. M. Jeon, S. J. Lee, Y. Jang, D. Y. Cho, C. S. Hwang, *Nanotechnology* **2018**, *29*, 155203.
- [12] I. J. Kim, M. K. Kim, J. S. Lee, *Appl. Phys. Lett.* **2022**, *121*, 042901.
- [13] S. Jeong, Y. G. Ha, J. Moon, A. Facchetti, T. J. Marks, *Adv. Mater.* **2010**, *22*, 1346.
- [14] J. Sheng, T. Hong, H. M. Lee, K. Kim, M. Sasase, J. Kim, H. Hosono, J. S. Park, *ACS Appl. Mater. Interfaces* **2019**, *11*, 40300.
- [15] S. Y. Lee, D. H. Kim, E. Chong, Y. W. Jeon, D. H. Kim, *Appl. Phys. Lett.* **2011**, *98*, 122105.
- [16] M. H. Cho, C. H. Choi, H. J. Seul, H. C. Cho, J. K. Jeong, *ACS Appl. Mater. Interfaces* **2021**, *13*, 16628.
- [17] T. Kamiya, K. Nomura, H. Hosono, *Sci. Technol. Adv. Mater.* **2010**, *11*, 044305.
- [18] T. C. Chen, T. C. Chang, T. Y. Hsieh, C. T. Tsai, S. C. Chen, C. S. Lin, M. C. Hung, C. H. Tu, J. J. Chang, P. L. Chen, *Appl. Phys. Lett.* **2010**, *97*, 112104.
- [19] J. Y. Bak, Y. Kang, S. Yang, H. J. Ryu, C. S. Hwang, S. Han, S. M. Yoon, *Sci. Rep.* **2015**, *5*, 7884.
- [20] J. Zhang, J. G. Lu, Q. J. Jiang, B. Lu, X. H. Pan, L. X. Chen, Z. Z. Ye, X. F. Li, P. J. Guo, N. J. Zhou, *J. Vac. Sci. Technol. B* **2014**, *32*, 010602.
- [21] W. D. Xu, G. Q. Zhang, X. J. Feng, *Appl. Surf. Sci.* **2022**, *578*, 151987.
- [22] K. Woo, S. H. Lee, S. Lee, S. Y. Bak, Y. J. Kim, M. Yi, *Microelectron. Eng.* **2019**, *215*, 111006.
- [23] J. H. Jeon, Y. H. Hwang, B. S. Bae, H. L. Kwon, H. J. Kang, *Appl. Phys. Lett.* **2010**, *96*, 212109.
- [24] S. Lee, M. Kim, G. Mun, J. Ko, H. I. Yeom, G. H. Lee, B. Shong, S. H. K. Park, *ACS Appl. Mater. Interfaces* **2021**, *13*, 40134.
- [25] W. D. Xu, M. Xu, J. F. Jiang, C. N. Luan, L. Han, X. J. Feng, *IEEE Electron Device Lett.* **2019**, *40*, 247.
- [26] J. I. Park, Y. Lim, M. Jang, S. I. Choi, N. Hwang, M. Yi, *Mater. Res. Bull.* **2017**, *96*, 155.
- [27] T. H. Cheng, S. P. Chang, S. J. Chang, *J. Electron. Mater.* **2018**, *47*, 6923.
- [28] H. B. Profijt, S. E. Potts, M. C. M. van de Sanden, W. M. M. Kessels, *J. Vac. Sci. Technol. A* **2011**, *29*.
- [29] D. H. Lee, D. G. Kim, M. Kim, S. Uhm, T. Kim, B. Kuh, J. S. Park, *ACS Appl. Electron. Mater.* **2022**, *4*, 5608.
- [30] J. Z. Sheng, J. H. Lee, W. H. Choi, T. Hong, M. Kim, J. S. Park, *J. Vac. Sci. Technol. A* **2018**, *36*.
- [31] J. B. Ko, S. H. Lee, K. W. Park, S. H. K. Park, *RSC Adv.* **2019**, *9*, 36293.
- [32] Y. K. Moon, S. Lee, W. S. Kim, B. W. Kang, C. O. Jeong, D. H. Lee, J. W. Park, *Appl. Phys. Lett.* **2009**, *95*, 013507.
- [33] A. Abliz, *J. Alloys Compd.* **2020**, *831*, 154694.
- [34] Y. Nam, H. O. Kim, S. H. Cho, S. H. K. Park, *RSC Adv.* **2018**, *8*, 5622.
- [35] S. I. Cho, J. B. Ko, S. H. Lee, J. Kim, S. H. K. Park, *J. Alloys Compd.* **2022**, *893*, 162308.
- [36] S. I. Cho, J. B. Jeon, J. H. Kim, S. H. Lee, W. Jeong, J. Kim, G. Kim, K. M. Kim, S. H. K. Park, *J. Mater. Chem. C* **2021**, *9*, 10243.

- [37] W. H. Choi, K. Kim, S. G. Jeong, J. H. Han, J. Jang, J. Noh, K. S. Park, J. J. Kim, S. Y. Yoon, W. Jeon, J. S. Park, *IEEE Trans. Electron Device* **2021**, 68, 6147.
- [38] M. Bae, D. Yun, Y. Kim, D. Kong, H. K. Jeong, W. Kim, J. Kim, I. Hur, D. H. Kim, D. M. Kim, *IEEE Electron Device Lett.* **2012**, 33, 399.
- [39] K. Ide, K. Nomura, H. Hosono, T. Kamiya, *Phys. Status Solidi A* **2019**, 216.
- [40] J. Sheng, H. J. Lee, S. Oh, J. S. Park, *ACS Appl. Mater. Interfaces* **2016**, 8, 33821.
- [41] Z. Z. Ye, S. L. Yue, J. Zhang, X. F. Li, L. X. Chen, J. G. Lu, *IEEE Trans. Electron Device* **2016**, 63, 3547.
- [42] M. J. Park, J. Y. Bak, J. S. Choi, S. M. Yoon, *ECS Solid State Lett.* **2014**, 3, Q44.
- [43] S. M. Park, D. H. Lee, Y. S. Lim, D. K. Kim, M. Yi, *Microelectron. Eng.* **2013**, 109, 189.
- [44] W. D. Xu, J. F. Jiang, L. Han, X. J. Feng, *Ceram. Int.* **2020**, 46, 17295.
- [45] M. Y. Liu, F. Qin, M. Rothschild, Y. X. Zhang, D. H. Lee, K. No, H. W. Song, S. Lee, *J. Electron. Mater.* **2022**, 51, 1813.